SCIENCE CHINA
Chemistry

•ARTICLES•

January 2022 Vol.65 No.1: 170–181
https://doi.org/10.1007/s11426-021-1079-5

FeOOH photo-deposited perylene linear polymer with accelerated charge separation for photocatalytic overall water splitting

Haonan Ye[1†], Zhiqiang Wang[2†], Ke Hu[3], Wenjun Wu[1], Xueqing Gong[2] & Jianli Hua[1*]

[1]*Key Laboratory for Advanced Material, Feringa Nobel Prize Scientist Joint Research Center, School of Chemistry and Molecular Engineering, East China University of Science and Technology, Shanghai 200237, China;*
[2]*Key Laboratory for Advanced Materials, Centre for Computational Chemistry and Research Institute of Industrial Catalysis, School of Chemistry and Molecular Engineering, East China University of Science and Technology, Shanghai 200237, China;*
[3]*Department of Chemistry, Fudan University, Shanghai 200433, China*

Received May 6, 2021; accepted July 26, 2021; published online November 3, 2021

It is a challenge to develop single polymer-based photocatalyst for overall water splitting without adding sacrificial agents due to the insufficient driving force for charge separation and the lack of active sites of organic polymer. Metal oxyhyroxides are widely acted as co-catalyst for photoelectrocatalysis oxygen evolution reaction. Here, we firstly report the peryleno[1,12-bcd] thiophene sulfone-based linear co-polymer **PS-5** for photocatalytic overall water splitting by photo-depositing simple and low-cost co-catalyst FeOOH under the visible-light illumination. The density functional theory (DFT) calculations and experimental results indicated clearly that the oxygen vacancies-rich β-FeOOH can effectively promote the separation of photo-generated excitons and provide active sites for photocatalytic oxygen evolution reaction. As a result, the average H_2 and O_2 production rates of optimized **PS-5/β-FeOOH-0.2M** reach at ~170 and ~76.6 μmol h^{-1} g^{-1}, respectively, with a stoichiometric ratio at about 2:1. This work provides a simple and low-cost method for the preparation of overall water splitting system based on polymer photocatalyst.

photocatalysis, conjugated polymers, FeOOH, photo-deposited, overall water splitting

Citation: Ye H, Wang Z, Hu K, Wu W, Gong X, Hua J. FeOOH photo-deposited perylene linear polymer with accelerated charge separation for photocatalytic overall water splitting. *Sci China Chem*, 2022, 65: 170–181, https://doi.org/10.1007/s11426-021-1079-5

1 Introduction

Utilizing semiconductor photocatalysts and solar energy to split water into hydrogen and oxygen is a potential strategy for sustainable development [1–4]. In the development of photocatalytic materials for decades, most semiconductors employed for water splitting are inorganic materials [5–8]. Recently, since graphite phase carbon nitride (GCN) is innovatively regarded as photocatalyst [9–11], the low-cost organic polymers with mild preparation method and adjustable structure have emerged as potential semiconductors for photocatalytic water splitting and great progress has been made in these fields [12–18]. Unfortunately, organic polymers often suffer from large exciton binding energy [19–21], and inability to transfer four oxidative equivalents for efficient water oxidation [22,23]. Hence, the applications of various organic polymers are mostly limited in semi-reactions of photocatalytic hydrogen evolution, and depend on the use of sacrificial agents (*i.e.*, triethanolamine or triethylamine) [24,25]. The development of single polymer for overall water splitting has become a challenge, because the few polymers win both narrow band gap to absorb visible light and enough over-potential to drive photocatalytic half reaction. Thus, much effort has been attempt to enhance the charge separation ability of organic polymer semiconductors

†These authors contributed equally to this work.
*Corresponding author (email: jlhua@ecust.edu.cn)

[26,27], such as the construction of multicomponent Z-scheme inspired by the photosynthesis system in nature [5,28,29]. Although some pioneering work on all organic Z-scheme has achieved efficient and stable activity of photocatalytic overall water-splitting [30,31], the relevant report is still very few due to its complex and difficult preparation.

Therefore, polymer-cocatalyst multicomponent hybrids are urgently needed for large scale, highly efficient water splitting system. However, most co-catalysts employed to reducing over-potential for photocatalytic reaction are noble metals [32,33], which is detrimental to scale-up production. Lately, the VIII metal oxyhyroxides, such as FeOOH, NiOOH, are widely acted as co-catalyst for photoelectrocatalysis oxygen evolution reactions (OER) owing to its low cost and high efficiency [34,35]. Among them, the oxygen vacancies-rich FeOOH can capture and store photogenerated holes, and drive the efficient separation of electrons and holes [36]. Moreover, the FeOOH can provide catalytic active sites and effectively reduce the over-potential of oxygen evolution. For instance, Bi *et al*. [37] have grown ultra-thin FeOOH nano-crystalline (2 nm) on $BiVO_4$ photoanodes *via* a simple solution immersion strategy, and the modified photoanodes achieved efficient water oxidation with an extraordinary photocurrent density. And Kang *et al*. [35] accidentally discovered that the *in-situ* generated FeOOH on cobalt perylene diimide nanocrystal remarkably benefit for quick electron-hole separation, and the optimized semiconductors obtained the record value of photocatalytic water oxidation rates (27,000 μmol g^{-1} h^{-1}).

In our previous work, a novel peryleno[1,12-bcd] thiophene sulfone-based conjugated co-polymer **PS-5** with wide absorption spectrum and excellent charge separation ability has been reported for highly efficient photocatalytic hydrogen production [38]. Hence, in this work, we further explore its application in overall water splitting, in which β-FeOOH is employed as the co-catalyst for OER. As shown in Figure 1, the β-FeOOH is loaded on the surface of polymer evenly by a simple photo-deposition method in the precursor of $FeCl_2$ aqueous solution. Subsequently, the photocatalytic performance of the as-prepared samples is tested and the influence of photo-deposited β-FeOOH on photocatalytic activity is further explored by photoelectrochemical experiments. Upon visible-light illumination, the optimized **PS-5/β-FeOOH** composite exhibits excellent photocatalytic performance for overall water splitting without any sacrificial agent adding, owing to its following characteristics: (1) the polymer **PS-5** possesses both the strong visible light absorption capacity and suitable energy level for overall water splitting; (2) the oxygen vacancies-rich β-FeOOH can effectively capture photo-generated holes and promote the separation of excitons; (3) the β-FeOOH can provide active sites for photocatalytic OER. As results, the average H_2 and O_2 production rates of optimized **PS-5/β-FeOOH-0.2M** reach at ~170 and ~76.6 μmol h^{-1} g^{-1}, respectively, with a stoichiometric ratio at about 2:1. Significantly, this is the first report using linear polymer to construct photocatalytic overall water splitting system by β-FeOOH photo-deposition route.

2 Experimental

2.1 Materials and measurements

The original compounds of dibenzo[b,d] thiophene 5,5-dioxide, perylene were commercially purchased and used directly. The intermediate compounds of 3,10-dibromoperyleno [1,12-bcd]thiophene 1,1-dioxide, 3,7-bis (4,4,5,5-tetramethyl-1,3,2-dioxaborolan-2-yl)dibenzo[b,d]

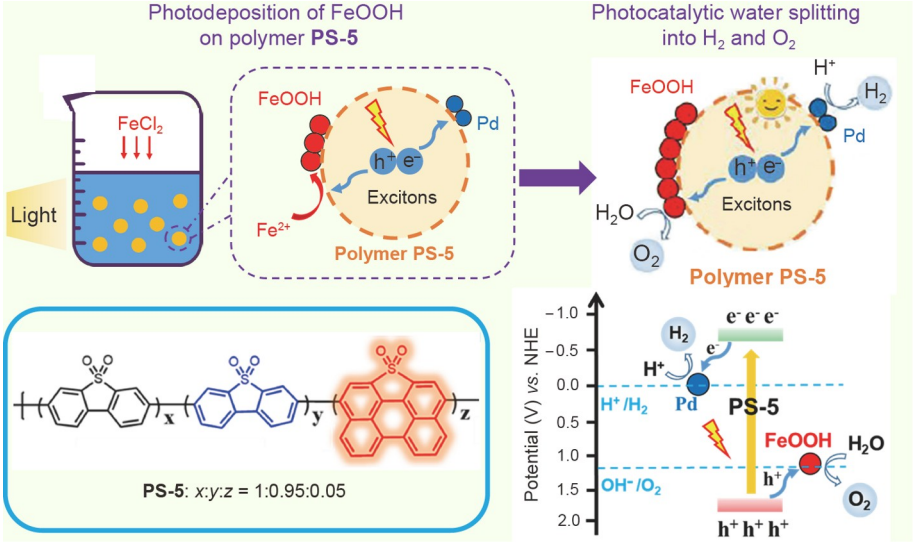

Figure 1 The mechanism diagram of photo-deposition of β-FeOOH on **PS-5** and overall water splitting of photocatalyst (color online).

thiophene 5,5-dioxide, and 3,7-dibromodibenzo[b,d] thiophene 5,5-dioxide were synthesized according to previous papers [38]. All other chemical reagents involved in the reaction were also purchased through commercial channels. All reactions were carried out in nitrogen atmosphere and all glasswares were dried in oven with high temperature.

The Fourier transform infrared (FTIR) spectra were measured on NIswew COLET 380 spectrometer (Thermo, USA) with a standard KBr pellet technique. Powder X-ray diffraction patterns (PXRD) was manipulated on a RigakuD/MAX 2550 diffract meter (Japan), and the test conditions are under 100 mA and 40 kV (Cu K radiation, λ=1.5406 Å). The time of flight-secondary ion mass spectrometry (TOF-SIMS) was measured on ToF-SIMS V (ION-TOF GmbH, Munster, Germany), and the test conditions are under current 1.2 pA and 30 keV Bi^+ primary ions at positive mode, and the analysis areas are 100×100 μm^2, 128×128 pixels, cycle time 100 μs, 100 scans. X-ray photoelectron spectroscopy (XPS) data were acquired on a Perkin-Elmer PHI 5000C ESCA system (USA), the test condition is at 250 W (Al Kα radiation). All binding energies were based on the C 1s peak (284.6 eV). High resolution transmission electron microscopy (HRTEM) spectra were recorded on the JEM-2100EX to obtain the sample morphologies. Diffuse reflectance spectroscopy (DRS) ultraviolet-visible (UV-vis) characterizations were obtained on a Varian Cary 500 spectrophotometer (USA). Photoluminescence (PL) spectrum was measured at room temperature on a Hitachi F-4500 fluorescence spectrophotometer (Japan). Specifically, the excitation wavelength of the PL emission spectra was 385 nm, and the time-resolved PL decay spectra were carried out at 410 nm for **PS-5**, and 415 nm for **PS-5/β-FeOOH-*X***. The value of the goodness-of-fit parameter (χ^2) is between 1 and 1.5, indicating good credibility of the calculated data in decay kinetics calculation.

2.2 Synthesis of polymers

The **PS-3**–**PS-5** polymers were synthesized by classical Suzuki polymerization of diboronic ester arenes and dibromo arenes, according to our previous work [38], and the synthetic route and the chemical structure of polymers are shown in Scheme 1.

2.3 Samples preparation

Preparation of **PS-5/β-FeOOH-*X*** composite: The ferric salts ($FeCl_2{\cdot}4H_2O$, $FeCl_3{\cdot}6H_2O$, $Fe(NO_3)_3{\cdot}4H_2O$, and $Fe_2(SO_3)_3$) were commercially purchased and used directly. 20 mg **PS-5** was uniformly dispersed in a 50 mL deionized water, and 10 mmol (5 or 20 mmol) $FeCl_2{\cdot}4H_2O$ was dropped into the dispersion solution. The dispersion solution was evenly stirred for 6 h under light irradiation (300 W Xe-lamp). The samples of **PS-5/β-FeOOH-0.2M** (**PS-5/β-FeOOH-0.1M** or **PS-5/β-FeOOH-0.4M**) were given after centrifugation, washing repeatedly and drying at 60 °C for 12 h. In addition, other ferric salts ($FeCl_3{\cdot}6H_2O$, $Fe(NO_3)_3{\cdot}4H_2O$ or $Fe_2(SO_3)_3$) were also employed as precursors to prepare corresponding samples for exploring the effect of iron valence or anion type on the photocatalytic activity of **PS-5/β-FeOOH** samples. The actual content of Fe loading by inductively coupled plasma optical emission spectrometer (ICP-OES) on **PS-5** is ~1.8 wt%, ~4.1 wt%, ~7.7 wt% for **PS-5/β-FeOOH-*X*** (*X*=0.1, 0.2, 0.4 M), respectively. And actual content of residual Pd loading is ~0.8 wt%, ~1.2 wt%, ~0.5 wt% for **PS-5/β-FeOOH-*X*** (*X*=0.1, 0.2, 0.4 M), respectively.

2.4 Electrochemical analysis

The Mott-Schottky plots, transient electrochemical impedance spectra (EIS) and photocurrent responses (*I-t*) of samples were also obtained on a CHI650E electrochemical workstation with a classic three-electrode system (Pt wire as counter electrode, and Ag/AgCl as the reference electrode). The working electrode preparation process is as follows: Mix 20 mg of samples and 10 μL of a Nafion (5%) aqueous solution with ethanol as solvent and grind into slurry. The slurry was uniformly coated on indium tin oxide (ITO)

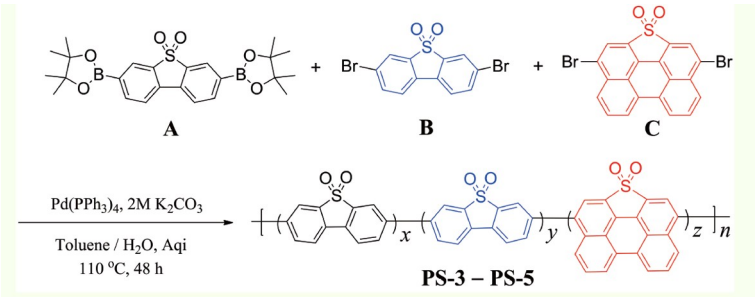

Monomer ratios	PS-3	PS-4	PS-5
x:*y*:*z*	1:1:0	1:0.975:0.025	1:0.95:0.05

Scheme 1 General synthetic routes of the **PS-3**–**PS-5** (color online).

glasses and the ITO glassed was fired at 120 °C for 1 h to obtain the desired working electrode. Mott-Schottky plots were collected at 1,000 MHz with a scan rate of 1 mV s^{-1}. The calculation formula of conduction band (CB) is: E_{CB} (normal hydrogen electrode (NHE), pH 7)=E_{fb} (Ag/AgCl, pH 7) + 0.197 − X. For n-type semiconductors, the fixed value of X is 0.2. The *I-t* measurements were performed with the light on and off (300 W Xe-lamp, $\lambda > 420$ nm) in a 0.5 M Na_2SO_4 aqueous solution, and the bias was 0 V *versus* Ag/AgCl. For EIS, the frequency range was 10^2–10^6 Hz and the amplitude was 10 mV at the open circuit voltage.

2.5 Photocatalytic activity measurement

The photocatalytic hydrogen evolution experiments were tested in a glass gas-closed-circulation system (CEL-SPFLU-DFBZN) connected to a gas chromatography (GC 2060, TCD detector, and Ar carrier) under 300 W xenon lamp (CEL-HXF 300) irradiation. And the temperature of the reaction solution was controlled at about 303 K by a flow of circling water connected to thermo-control devices.

Photocatalytic H_2 evolution test. 20 mg sample of **PS-5** or **PS-5/FeOOH-*X*** dispersing in deionized water solution with 20 vol% triethanolamine as sacrificial agent was employed to photocatalytic test. Before the test, the whole device was first vacuumed by a vacuum pump, and photocatalytic reactor was then placed under visible-light illumination (300 W xenon lamp, 420 nm ≤ λ ≤ 780 nm) for testing.

Photocatalytic O_2 evolution test. 20 mg sample of **PS-5** or **PS-5/FeOOH-*X*** dispersing in deionized water solution with 100 mg $AgNO_3$ as the sacrificial agent and 100 mg La_2O_3 as a pH buffer agent was employed to photocatalytic test. Before the test, the whole device was first vacuumed by a vacuum pump, and photocatalytic reactor was then placed under visible-light illumination (300 W xenon lamp, 420 nm ≤ λ ≤ 780 nm) for testing.

Photocatalytic overall water splitting. Photocatalytic overall water splitting reaction was carried out by dispersing 20 mg of photocatalysts power into 50 mL deionized water under the irradiation of a 300 W Xe lamp (300 W xenon lamp, 420 nm ≤ λ ≤ 780 nm).

AQY measurement. AQY measurement for overall water splitting was performed under at monochromatic light irradiation (300 W xenon lamp, λ=420, 435, 475, 500, 520, 550, 630 nm). 20 mg sample was dispersed in deionized water. The calculation formula of AQY was estimated as

$$\text{AQY}\ (\%) = \frac{2\times\text{Number of evolved } H_2 \text{ molecules}}{\text{Number of incident photons}} \times 100\% = (2C \cdot NA)(h \cdot c) / (S \cdot P \cdot t \cdot \lambda) \times 100\%$$

where C is the hydrogen evolution amount (μmol) per hour; NA is the Avogadro constant (6.022×10^{23} mol^{-1}); S is the illumination area (12.56 cm^2); P is the light intensity; t is the illumination time (3,600 s); λ is the wavelength of the monochromatic light (m); h is the Plank constant (6.626×10^{-34} J s); c is the speed of light (3×10^8 m s^{-1}).

2.6 Density functional theory computational methodology

Density functional theory (DFT) calculations were performed with the Vienna Ab-initio Simulation Package (VASP) [39]. In our calculations, the spin-polarized projector augmented wave (PAW) methods were applied together with the Perdew-Burke-Ernzerhof (PBE) electron exchange correlation functional of the generalized gradient approximation (GGA) [40–42]. The energy cut-off of the wave function in the plane-wave basis was set to 400 eV, the calculations were carried out until the maximum force upon each relaxed atom was less than 0.05 eV $Å^{-1}$. To optimize the polymer **PS-5** and FeOOH systems, the unit cell is set to 40 Å×40 Å×20 Å to avoid the interactions between the neighbouring systems, and a Monkhorst-Pack grid of (1×1×1) k points was used, all atoms in these systems were allowed to relax.

3 Results and discussion

3.1 Synthesis

According to our previous work, the novel peryleno[1,12-bcd] thiophene sulfone-based conjugated co-polymer **PS-5** showed remarkable performance photocatalytic hydrogen generation, due to its wide absorption spectrum and excellent charge separation ability [38]. In order to further enhance its electron-holes separation and subsequently explore its application in overall water splitting, the co-catalyst β-FeOOH for OER was photo-deposited on the surface of co-polymer **PS-5**. In more detail, the HO-Fe(II)-OH was formed *via* the coordination of Fe^{2+} and H_2O, and then OER cocatalyst O=Fe(III)-OH was the produced immediately and nucleates uniformly on surface of **PS-5** after the HO-Fe(II)-OH was oxidized by the photo-generated holes. And the residual palladium from Pd (0)-catalyzed suzuki polymerization was employed as co-catalyst for hydrogen evolution in this work.

The chemical composition, crystal structure and surface morphology of obtained **PS-5/β-FeOOH** photocatalysts were characterized by FTIR (Figure 2a), XPS (Figure 2b–d), TOF-SIMS (Figure 2e, f), PXRD (Figure 3a), EDS-mapping (Figure 3b), and HRTEM (Figure 3c–f), respectively. The preparation method of this polymer-cocatalyst multicomponent hybrid and the corresponding characterization technology was specifically described in the experimental section, and the mechanism diagram was shown in Figure 4c.

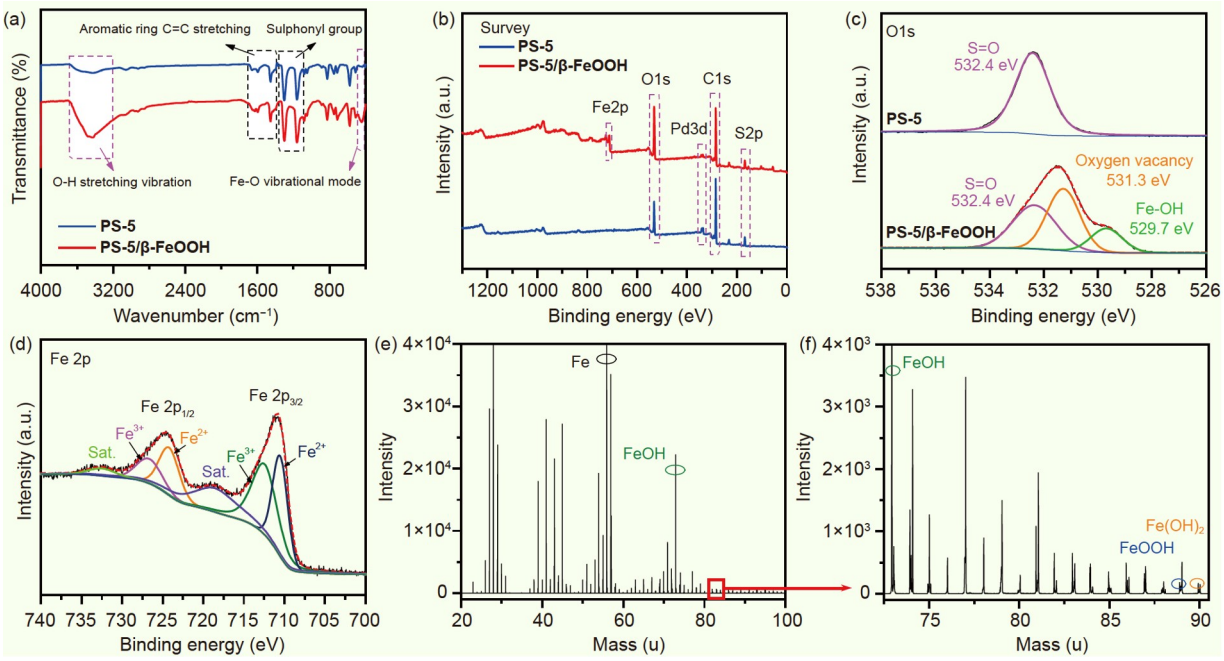

Figure 2 (a) FTIR spectra of **PS-5** and **PS-5/β-FeOOH**. High-resolution XPS spectra of **PS-5** and **PS-5/β-FeOOH** composite materials: (b) survey; (c) O 1s; (d) Fe 2p. (e, f) The TOF-SIMS spectrogram of **PS-5/β-FeOOH** (color online).

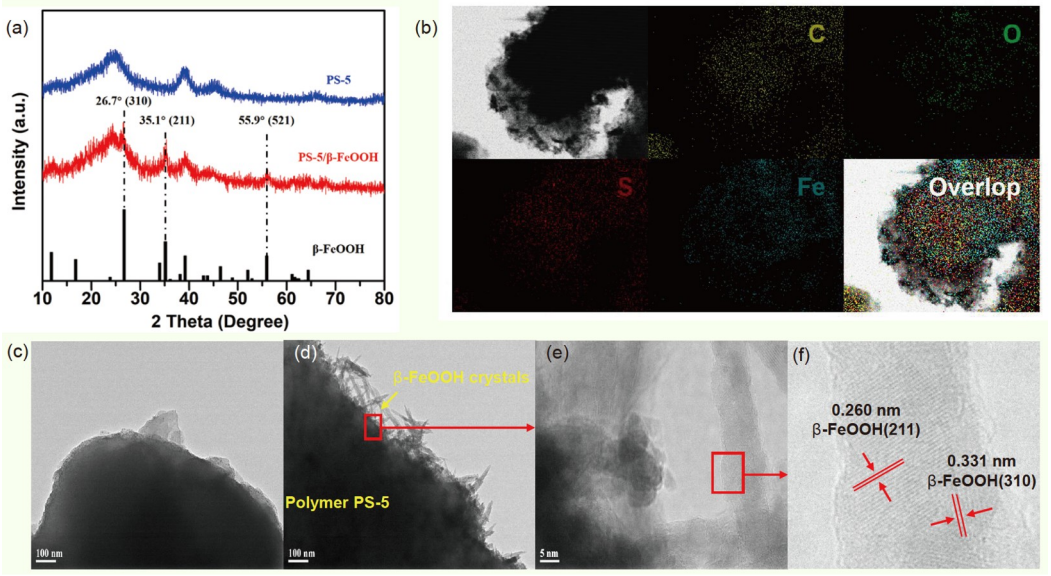

Figure 3 (a) PXRD spectra of **PS-5** and **PS-5/β-FeOOH**. (b) TEM-EDS elemental mapping images of **PS-5/β-FeOOH**. HRTEM images of **PS-5** (c) and **PS-5/β-FeOOH** (d–f). Scan bar: 100 nm (color online).

3.2 Structural and morphological characterization

The chemical structures of prepared **PS-5/β-FeOOH** samples were characterized by FTIR, TOF-SIMS and XPS. As shown in Figure 2a, the sharp vibration peak at around 1,600, 1,140 and 1,315 cm^{-1} for all samples were attributed to the aromatic ring C=C stretching vibrations and O=S=O group, respectively [43], indicating that the framework structure of the **PS-5** was kept intact during photo-deposition of β-FeOOH. Compared with **PS-5**, the stronger peak at around 3,400 cm^{-1} and the emerging peak at around 430 cm^{-1} were found for **PS-5/β-FeOOH**, which were assigned to O–H and Fe–O bonds, respectively [44], confirming the deposition of FeOOH on the surface of polymer.

XPS spectra employed to get insight the surface electron composition and element structure, provided more in-

formation about possible chemical bonds formed in **PS-5/β-FeOOH** materials. Seen from Figure 2b and Table S1 (Supporting Information online), the main elements of pure **PS-5** and as-prepared **PS-5/β-FeOOH** were carbon (C), oxygen (O), sulfur (S) and palladium (Pd). In addition, lower C/O ratio and emerging iron (Fe) were observed in **PS-5/β-FeOOH** sample owing to the existence of FeOOH (Table S1). The Figure 2c, d and Figure S1 (Supporting Information online) exhibited the high-resolution C 1s, S 2p, O 1s and F 2p XPS spectra of pure **PS-5** and as-prepared **PS-5/β-FeOOH** compound materials. Firstly, as shown in Figure S1, the C 1s and S 2p spectra of the samples showed no obvious change before and after FeOOH loading, where their binding energies at around 284.6 and 168 eV belong to C=C and C-SO_2-C, respectively, indicating that the skeleton structures of polymers have not been destroyed. In addition, compared with pure **PS-5** sample, except for binding energy at around 532.4 eV corresponding to S=O, two new peaks in binding energy at 529.7 and 531.3 eV in high-resolution O 1s of **PS-5/β-FeOOH** were assigned to the F–OH bonds and oxygen vacancies, respectively (Figure 2c) [37]. It was also found that both Fe^{3+} and Fe^{2+} were present within the range of 730 to 710 eV in Fe 2p of **PS-5/β-FeOOH** (Figure 2d). Furthermore, TOF-SIMS was utilized to prove the formation of FeOOH on polymer *via* photo-deposition method. As shown in Figure 2e, f, the Fe^{+}-signal, Fe-OH^{+}-signal, $FeOOH^{+}$-signal and $Fe(OH)_2^{+}$-signal could be clearly found in as-prepared **PS-5/β-FeOOH** films, confirming the FeOOH has already generated on **PS-5**. All these results indicated that the loading of FeOOH on polymer **PS-5** and the cycle reaction of Fe^{2+} and Fe^{3+} occurred during the photo-deposition process.

The crystal structures of **PS-5** and **PS-5/β-FeOOH** were further characterized by PXRD. Seen from Figure 3a, all samples showed the same humps at around 25.0° and 40.0° in PXRD pattern, which belonged to the typical π-π stacking between the polymer backbones, implying the amorphous structure of polymers and the frameworks of polymers were not destroyed during the photo-deposition process. In addition, it is worth noting that there were some new sharp peaks showing up at 26.7°, 35.1° and 55.9° for **PS-5/β-FeOOH** samples. Those new peaks could be well indexed to the (310), (211) and (521) facet of β-FeOOH (PDF card #34-1266), confirming the existence of β-FeOOH in as-prepared photocatalyst. The more direct morphology information of the samples was obtained in HRTEM images. As shown in Figure 3c, the **PS-5** without β-FeOOH loading exhibited wide range of amorphous structure. For **PS-5/β-FeOOH** samples, we observed that the irregular amorphous structure of polymer had no obvious change (Figure 3d), suggesting the morphology of polymer was retained. Besides, there was obvious needle-like crystal loading on the surface of the polymer in **PS-5/β-FeOOH** samples. And the well-resolved lattice fringes of 0.260 and 0.331 nm were observed in the high-resolution TEM image in Figure 3f. Those lattice fringes were corresponding to the (211) and (310) planes of β-FeOOH [34], which was consistent with result of PXRD. Furthermore, as shown in element mapping image in Figure 3b and Figure S2, it illustrated the existence of C, O, S, Fe and Pd elements in the whole regions, further suggesting the uniform distribution of β-FeOOH on polymer surface. All these results indicated that β-FeOOH could uniformly nucleate on the surface of polymers by photo deposition without destroying the structure of polymer.

3.3 Optical properties characterization and energy level

The influence of β-FeOOH loading on the optical properties of the photocatalytic materials was investigated by UV-vis DRS. As shown in Figure 4a, due to the presence of extended π-conjugation for peryleno[1,12-bcd]thiophene sulfone in polymer skeleton, the organic polymer photocatalyst **PS-5** exhibited remarkable visible-light absorption range even up to 600 nm, which benefits for absorbing a large number of photons and produces abundant photo-generated excitons to further participate in the photocatalytic reaction. After the photo-deposition of β-FeOOH, the UV-vis absorption spectra of **PS-5/β-FeOOH** samples did not change significantly compared with **PS-5**, suggesting the loading of β-FeOOH did not affect apparently the visible-light absorption activity of the **PS-5**. Moreover, the optical band gaps (E_g) of **PS-5** and **PS-5/β-FeOOH** determined from Tauc plots were both 2.12 eV *vs*. NHE.

The conduction band (CB) of photocatalysts was detected by Mott-Schottky plots on a CHI650E electrochemical workstation with a classic three-electrode system (photocatalyst film on ITO glasses as working electrode, Pt wire as counter electrode, and Ag/AgCl as reference electrode) in 0.5 M Na_2SO_4 aqueous solution. The calculation formula of CB is: E_{CB} (NHE, pH 7)=E_{fb} (Ag/AgCl, pH 7)+0.197−X. As shown in Figure 4b, the positive slope of Mott-Schottky plots for all samples indicated that the photocatalysts were classic n-type semiconductors and the fixed value of X was 0.2 in this work [45]. The CB of **PS-5** and **PS-5/β-FeOOH** were both calculated at −0.49V *vs*. NHE. The valence band (VB) edge was estimated by adding the E_g value to the CB edge to be 1.63 eV for **PS-5**, and the corresponding energy levels of polymers were shown in Figure 4c. Notably, **PS-5** and **PS-5/β-FeOOH** showed similar energy level structure, indicating the FeOOH was only employed as OER cocatalyst in our work. The CB of **PS-5** lies higher in energy level than the H_2O/H_2 redox potential (0 V *vs*. NHE), and the VB of **PS-5** is lower than H_2O/O_2 redox potential (1.23 V *vs*. NHE), suggesting that the photocatalyst **PS-5** has potential application in photocatalysitc overall water splitting.

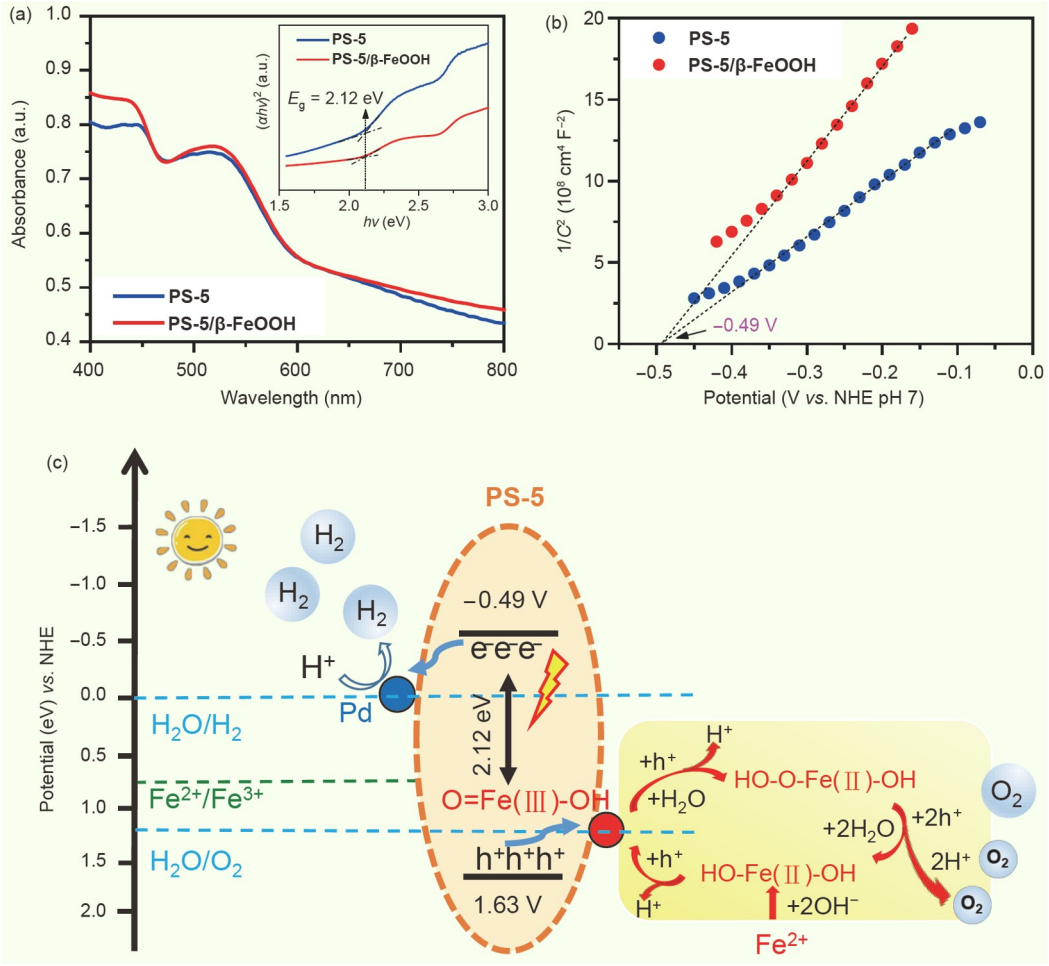

Figure 4 (a) UV-vis absorption spectra of **PS-5** and **PS-5/β-FeOOH** (inset shows the Tauc-plots of **PS-5** and **PS-5/β-FeOOH**). (b) Mott-Schottky plots of **PS-5** and **PS-5/β-FeOOH**. (c) Schematics of the relative positions of energy level for **PS-5** and the corresponding photocatalytic water splitting process (color online).

3.4 Computational and photo-electrochemical studies

For most organic photocatalysts, the large exciton binding energy limits the improvement of its photocatalytic activity, and hence lots of work has been done to enhance the charge separation and transfer ability of polymer semiconductor. In this work, the polymer-cocatalyst multicomponent hybrid was successfully constructed, and the DFT calculations with VASP were employed to provide insights into the interface charge distribution between polymer and FeOOH.

Firstly, the Bader charge analyses for the charge distribution of **PS-5** and **PS-5/FeOOH** were carried out to quantify the charge separation intuitively. Figure 5 exhibited the side and top views of simulation models of **PS-5** and **PS-5/FeOOH** cluster, respectively. As shown in Figure 5a, due to the introduction of peryleno[1,12-bcd]thiophene sulfone unit with excellent flatness, the effective charge separation existed in the polymer backbone, and the peryleno[1,12-bcd] thiophene sulfone unit processed the maximum value of Bader charge (0.067 |e|). After loading FeOOH onto the polymer surface, the Bader charge of monomer units in polymer rearranged (Figure 5b). Particularly, the Bader charge of peryleno[1,12-bcd]thiophene sulfone unit close to the FeOOH cluster converted to negative value (−0.345 |e|), indicating the electron transfer to peryleno[1,12-bcd]thiophene sulfone unit happened. In addition, charge redistribution occurs at the interface between polymer **PS-5** and FeOOH. In the system of **PS-5/FeOOH** composite, the Bader charge of **PS-5** and FeOOH were −0.314 |e| and 0.314 |e|, which represented the electron and holes accumulated in **PS-5** and FeOOH, respectively. Therefore, because the oxygen vacancies-rich β-FeOOH can effectively capture holes [37], we speculate that a polarized in-built electric field (IEF) in the direction of FeOOH to **PS-5** is established, which can effectively inhibit the charges recombination, accelerate the separation of photo-generated charges and consequently is beneficial for photocatalytic water-splitting.

Subsequently, to further prove this speculation, the transient photocurrent responses (*I*-*t*) and EIS were employed to investigate the influence of the introduction of FeOOH on

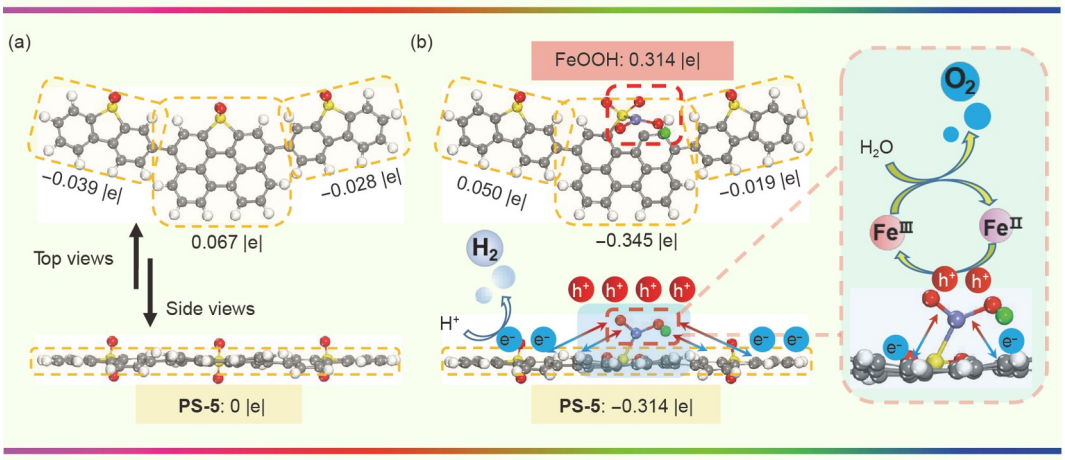

Figure 5 Calculated Bader charges for **PS-5** (a), **PS-5/FeOOH** (b) and illustration of the charge transfer between **PS-5** and FeOOH interface. The red arrows symbolize the holes transfer, while the blue arrows symbolize the electron transfer. White balls are H atoms in polymers, grey balls are C, yellow balls are S, red balls are O, purple balls are Fe, and green balls are H in FeOOH (color online).

the electron-hole separation and transfer of as-prepared photocatalyst samples. These measurements were carried out in a traditional three electrode system, in which the preparation method of the working electrode was described in the experimental section. As illustrated in Figure 6a, the good correlation between *I-t* curves and on-off cycles of samples (**PS-5** and **PS-5/β-FeOOH**) upon intermittent visible-light illuminate was found, indicating all samples possess superior photoactivity. The relatively lower photocurrent density was detected for **PS-5** loading at ~1.0 μA cm^{-2}. After photo-deposition of FeOOH on polymer, the photocurrent density of **PS-5/β-FeOOH** achieved quadruple enhancement at ~4.0 μA cm^{-2}. Furthermore, the EIS measurement was utilized to test the charge transfer rate of as-prepared samples. As shown in Figure 6b, after the FeOOH was loaded on **PS-5**, the semicircle of **PS-5/β-FeOOH** significantly reduced radius in Nyquist plots. In general, higher photocurrent density in *I-t* curves and decreased radius in EIS measurement always means faster charge transfer capability for photocatalyst. In this work, the introduction of FeOOH can effectively enhance the charge mobility of photocatalyst.

The PL spectroscopy of as-prepared samples was used to measure the charge transfer kinetics of photocatalysts. Seen from Figure 6c, the **PS-5** in tetrahydrofuran (THF) solution exhibited strong fluorescence peak at 410 nm because of the strong charge recombination. After FeOOH loading, the fluorescence quenching of photocatalyst was observed. The fluorescence peak with reduced intensity and red shift was detected for **PS-5/β-FeOOH** at 415 nm, indicating the charge recombination was effectively suppressed and quick charge transfer occurred. Moreover, the time-resolved fluorescence spectroscopy (TRFS) was employed to characterize the fluorescence lifetime of the photocatalyst. According to the literature [46], there was a negative correlation between the fluorescence lifetime and charge transfer activity. As shown in Figure 6d, compared with **PS-5** (1.03 ns), the fluorescence lifetimes (τ) of **PS-5/β-FeOOH** were 0.95 ns, confirming the efficient charge mobility in photocatalyst with β-FeOOH loading. In addition, the decay spectra of the samples can be fitted into two lifetime steps of $\tau 1$ and $\tau 2$, in which $\tau 1$ corresponds to the radiative lifetime (recombination process), and $\tau 2$ reflects the non-radiative lifetime of charge carriers (utilization process) [47–49]. The relative proportion of charge carriers (Rel.%) involved in the two steps were also listed in Table S2. The Rel.% of **PS-5** decreased from 92.26% to 72.50% (**PS-5/β-FeOOH**) in the first step ($\tau 1$), while a nearly four-fold growth was detected from 7.73% (**PS-5**) to 28.50% (**PS-5/β-FeOOH**) in the second step ($\tau 2$). The significant growth in Rel.% involved in the second step indicates that obviously enhanced photogenerated carrier migration and utilization has been realized. To sum up, all these photo-electrochemical studies make clear the pivotal role of β-FeOOH in accelerating the electron-hole pairs separation and transfer, which would further be favourable for photocatalytic reaction process.

3.5 Possible photocatalytic mechanism

Therefore, according to the above experiments, we successfully prepared low-cost **PS-5/β-FeOOH** photocatalyst using simple photo-deposition method. The corresponding energy level diagram of photocatalyst is shown in Figures 4c and 5d, the CB and VB of **PS-5** are well suited for overall water splitting, and a possible photocatalysis mechanism involving charge transfer is proposed. Upon illumination, **PS-5** with broad spectrum absorption ability, absorbs a large number of photons and generates electrons and holes. The

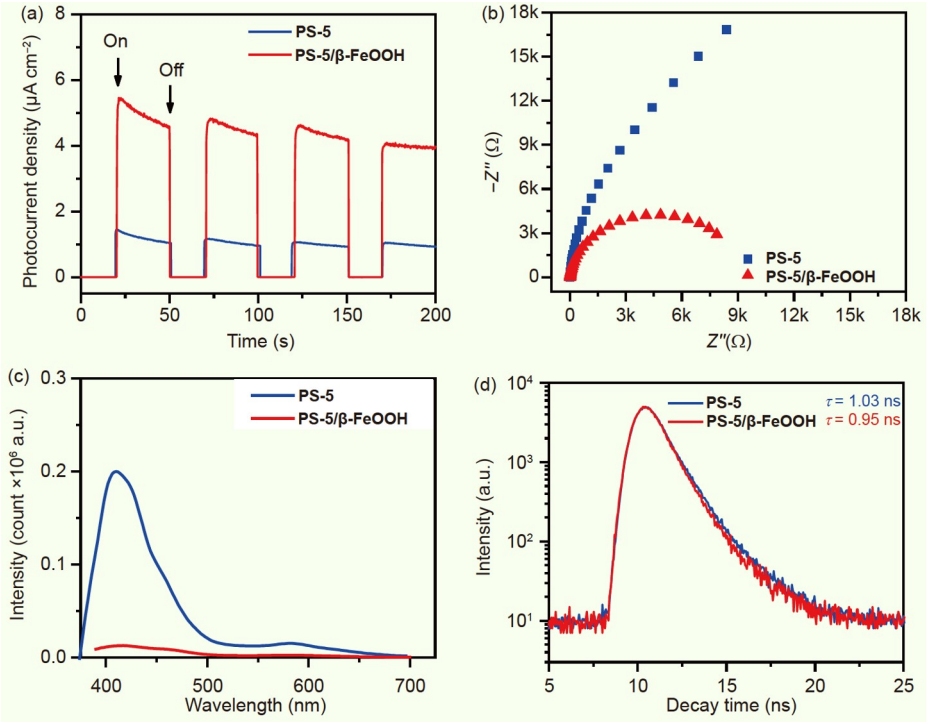

Figure 6 (a) Transient current responses to full time and on-off cycles photocurrent of illumination on **PS-5** and **PS-5/β-FeOOH** membrane electrodes. (b) EIS Nyquist plots of **PS-5** and **PS-5/β-FeOOH** membrane electrodes at open circuit voltage. (c) PL spectra of **PS-5** and **PS-5/β-FeOOH** in THF solution. (d) Time-resolved fluorescence spectroscopy of **PS-5** and **PS-5/β-FeOOH** in THF solution (color online).

photo-generated electrons jump into the CB of **PS-5**, transfer to the residual Pd during polymerization, and then reduce protons to produce hydrogen. In the meantime, the photo-generated holes transfer from the VB of **PS-5** to β-FeOOH, because the rich oxygen vacancies in β-FeOOH can effectively capture holes [37]. Thus, the HO-Fe (II)-OH is formed *via* the coordination of Fe^{2+} and H_2O, and then is oxidized by the holes immediately to produce O=Fe(III)-OH on the surface of **PS-5** [35,50,51]. Subsequently, O=Fe(III)-OH oxidizes the water to produce oxygen and HO-Fe(II)-OH, and then enters the next cycle of Fe^{2+} and Fe^{3+}, which is confirmed by results of the XPS and TOF-SIMS of **PS-5/β-FeOOH** (Figures 2 and 3). Therefore, in this mechanism, the β-FeOOH as co-catalyst for OER not only acts as catalytic active sites, but also accelerates the separation of excitons. Compared with **PS-5**, **PS-5/β-FeOOH** shows better charge separation efficiency, which is confirmed by generated in-built electric field (IEF), higher photocurrent response, lower charge transfer resistance, reduced PL intensity, and shorter PL decay lifetimes in photo-electrochemical studies above.

In addition, we further study the adsorption of water molecules on the surface of photocatalyst. Owing to the abundance of surface OH groups in FeOOH [52], the larger interface adhesion energy of the H_2O (E_{ads} (H_2O)) and smaller contact angle with water of **PS-5/FeOOH** indicate the better adsorption capacity for H_2O (Figure S3).

3.6 Photocatalytic activity and stability

Due to the good photo-response activity and suitable band structure of the as-prepared samples, we further explored the photocatalytic activity under visible-light irradiation. We firstly studied the water-half splitting reaction of as-prepared samples with sacrificial agent and further explored the influence of concentration of $FeCl_2$ precursor solution on the photocatalytic performance. The as-prepared samples were named as **PS-5/β-FeOOH-*X***, where *X* (*X*=0.1, 0.2, 0.4 M) is the concentration of $FeCl_2$ precursor solution. As shown in Figure 7a and Figure S4, for semi reaction of hydrogen production, upon visible-light illumination (420 nm ≤ λ ≤ 780 nm), the average amounts of hydrogen generation for **PS-5** (20 mg) was 178 μmol h^{-1} (8.9 mmol h^{-1} g^{-1}) in the presence of residual palladium as co-catalyst for HER and triethanolamine (TEOA) as the sacrificial agent. After the photo-deposition of β-FeOOH, with the increase of the concentration of the $FeCl_2$ precursor solution, the photocatalytic activity first increased and then decreased, and **PS-5/β-FeOOH-0.2M** obtained the highest HER at 204 μmol h^{-1} because the β-FeOOH accelerates the separation of photo-generated excitons. However, excessive catalyst deposition would act as the center of charge recombination, and the **PS-5/β-FeOOH-0.4M** with the lowest photocurrent response and the highest charge transfer resistance (Figures S6 and S7) exhibited the poorest activity

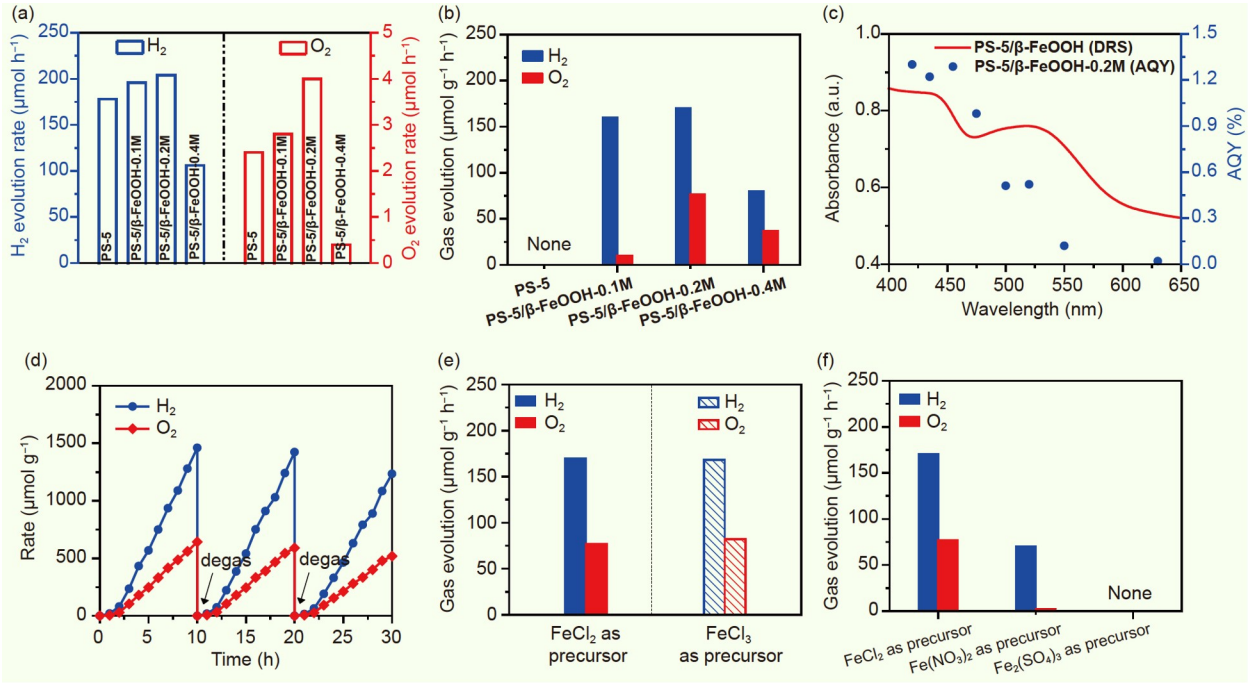

Figure 7 (a) Photocatalytic HER and OER semi-reaction of **PS-5** and **PS-5/β-FeOOH-*X*** (*X*=0.1, 0.2, 0.4 M) samples. (b) The photocatalytic overall water splitting activities of **PS-5** and **PS-5/β-FeOOH-*X***. (c) The wavelength dependent AQY of overall water splitting of **PS-5/β-FeOOH-0.2M**. (d) Cycling of photocatalytic overall water splitting of **PS-5/β-FeOOH-0.2M**. (e) The photocatalytic overall water splitting activities of **PS-5** and **PS-5/β-FeOOH** with 0.2 M $FeCl_2$ or $FeCl_3$ solution as precursor solution. (f) The photocatalytic overall water splitting activities of **PS-5** and **PS-5/β-FeOOH** with 0.2 M $FeCl_3$, $Fe(NO_3)_3$ or $Fe_2(SO_4)_3$ solution as precursor solution (color online).

of HER among four samples. The semi reaction of oxygen evolution was carried out in the presence of $AgNO_3$ as the sacrificial agent and La_2O_3 as a pH buffer agent (Figure 7a and Figure S5). Without β-FeOOH loading, the pure **PS-5** still obtained the detectable OER because its VB lied lower than the H_2O/O_2 redox potential. Similarly, the OER activities of the as-prepared samples with different concentrations of β-FeOOH loading showed the volcanic trend similar to HER. The **PS-5/β-FeOOH-0.2M** (20 mg) exhibited the highest OER at 4.0 μmol h^{-1} (200 μmol h^{-1} g^{-1}), which is 1.7 times of that of pure **PS-5**.

We further explored the performance of photocatalytic overall water splitting in pure deionized water under visible-light illumination (420 nm ≤ λ ≤ 780 nm) without any sacrificial agent adding, and the residual Pd of polymer reaction and β-FeOOH loading were employed as co-catalyst for HER and OER, respectively. As shown in Figure 7b and Figure S8, the HER and OER for pure **PS-5** were negligible, due to the strong exciton binding energy inside. After the photo-deposition of β-FeOOH, the ability of charge separation was enhanced, and the **PS-5/β-FeOOH-*X*** (*X*=0.1, 0.2, and 0.4 M) exhibited the detectable HER and OER. However, the stoichiometric ratio of hydrogen and oxygen production for **PS-5/β-FeOOH-0.1M** was much larger than 2:1 (H_2: 160 μmol h^{-1} g^{-1}; O_2: 10 μmol h^{-1} g^{-1}), owing to the insufficient loading of β-FeOOH [53]. As we expected, with the increasing amounts of β-FeOOH loading, the stoichiometric gas generation rates of H_2 and O_2 reached at 2:1. The **PS-5/β-FeOOH-0.2M** with accelerated charge separation and more catalytic sites obtained the highest photocatalytic activity up to 170 μmol h^{-1} g^{-1} for HER and 76.6 μmol h^{-1} g^{-1} for OER, respectively. Unfortunately, with further increased β-FeOOH loading, excessive catalyst deposition might lead to the lower charge separation ability (Figures S6 and S7), and reduced photocatalytic activity for **PS-5/β-FeOOH-0.4M**.

The AQY measurement for overall water splitting of **PS-5/β-FeOOH-0.2M** under various monochromatic light irradiations matched well with the absorption profile of as-prepared sample in DRS spectrogram (Figure 7c), suggestting that the HER and OER of **PS-5/β-FeOOH-0.2M** were driven by the visible light excitation. Furthermore, in the long-term stability test lasting for 30 h with each cycle of 10 h, there was no significant decrease of photocatalytic performance for **PS-5/β-FeOOH-0.2M** (Figure 7d). The samples were recovered after photocatalysis, and the FTIR, PXRD, HRTEM, XPS and DRS measurements of recovered sample after long-time test showed no apparent change compared with the as-prepared samples, indicating the high stability of structure and activity in the process of photocatalysis (Figures S9–S13). In addition, we prepared four batches of samples (**PS-5/β-FeOOH-0.2M**) and further explored the effect of Pd content on the photocatalytic activity. As shown in Figure S14, residual palladium was characterized by ICP-

OES, and their residual contents ranged from 0.51 wt% to 1.25 wt% for the photocatalysts. Notably, the amount of residual palladium was not directly related to the gas evolution rates of samples, indicating that the residual palladium had no obvious effect on the photocatalytic activity. To the best of our knowledge, this is the first report using linear polymers to construct photocatalytic overall water splitting systems by β-FeOOH photodeposition route.

We also investigated the effects of the valence of iron ions (Fe^{2+} or Fe^{3+}) and the type of anions (Cl^-, NO_3^- or SO_4^{2-}) in the precursor solution on the photocatalytic activity. As shown in Figure 7e and Figure S15, there was no obvious difference in properties between the samples prepared with $FeCl_2$ or $FeCl_3$ as precursor, because the Fe^{3+} ions could be immediately reduced to Fe^{2+} ions by photo-generated electrons, and further participate in the formation of β-FeOOH on the surface of **PS-5**. To our surprise, the samples prepared with $FeCl_3$ as precursor exhibited obvious and higher photocatalytic activity than those in $Fe(NO_3)_3$ or $Fe_2(SO_4)_2$ aqueous solution (Figure 7f). According to previous reports, in the process of photo-deposition using ferric salt as precursor liquid, smaller radius of anions and larger electronegativity were benefit for the formation of structurally stable β-FeOOH with high crystallinity [54]. Thus, the samples prepared with $FeCl_3$ as precursor obtained better crystallinity and higher photocatalytic activity (Figure S16). Moreover, our system can be applied to other polymers (PS-3 and PS-4) with appropriate energy level for overall water splitting and different pH test environments with stable photocatalytic performance, indicating the universality of this method (Figures S17–S19).

4 Conclusions

In summary, we have successfully developed the linear copolymers **PS-5/β-FeOOH** composite photocatalysts for overall water splitting without any sacrificial agent, in which the low-cost and efficient β-FeOOH co-catalyst for OER is loaded on **PS-5** by simple photo-deposition method. Among them, the average H_2 and O_2 production rates of optimized **PS-5/β-FeOOH-0.2M** reach at ~170 and ~76.6 μmol h^{-1} g^{-1}, respectively, with a stoichiometric ratio at about 2:1. The experimental results demonstrate that the non-noble metal co-catalyst β-FeOOH can be formed and uniformly nucleated on the polymer surface. The DFT calculations and experimental results indicate that the oxygen vacancies-rich β-FeOOH can act as catalytic active sites for OER and accelerate the separation and transportation of photo-generated excitons. This work provides a new and simple method for the design of polymers for overall water splitting system and broad prospect for the construction of multiple heterojunction system in the future.

Acknowledgements This work was supported by the National Natural Science Foundation of China (21788102, 21971064, 21772040), Shanghai Municipal Science and Technology Major Project (2018SHZDZX03), the Fundamental Research Funds for the Central Universities (222201717003, 50321101918001), and the Programme of Introducing Talents of Discipline to Universities (B16017). The authors thank Research Center of Analysis and Test of East China University of Science and Technology for the help on the characterization.

Conflict of interest The authors declare no conflict of interest.

Supporting information The supporting information is available online at http://chem.scichina.com and http://link.springer.com/journal/11426. The supporting materials are published as submitted, without typesetting or editing. The responsibility for scientific accuracy and content remains entirely with the authors.

1 Fabian DM, Hu S, Singh N, Houle FA, Hisatomi T, Domen K, Osterloh FE, Ardo S. *Energy Environ Sci*, 2015, 8: 2825–2850
2 Wang Z, Li C, Domen K. *Chem Soc Rev*, 2019, 48: 2109–2125
3 Safaei J, Mohamed NA, Mohamad Noh MF, Soh MF, Ludin NA, Ibrahim MA, Roslam Wan Isahak WN, Mat Teridi MA. *J Mater Chem A*, 2018, 6: 22346–22380
4 Gibson EA. *Chem Soc Rev*, 2017, 46: 6194–6209
5 Fujishima A, Honda K. *Nature*, 1972, 238: 37–38
6 Sun Q, Wang N, Yu J, Yu JC. *Adv Mater*, 2018, 30: 1804368
7 Wang X. *ChemSusChem*, 2018, 11: 327–329
8 Wang Q, Hisatomi T, Suzuki Y, Pan Z, Seo J, Katayama M, Minegishi T, Nishiyama H, Takata T, Seki K, Kudo A, Yamada T, Domen K. *J Am Chem Soc*, 2017, 139: 1675–1683
9 Wang X, Maeda K, Thomas A, Takanabe K, Xin G, Carlsson JM, Domen K, Antonietti M. *Nat Mater*, 2009, 8: 76–80
10 Lin L, Ou H, Zhang Y, Wang X. *ACS Catal*, 2016, 6: 3921–3931
11 Zhou BX, Ding SS, Zhang BJ, Xu L, Chen RS, Luo L, Huang WQ, Xie Z, Pan A, Huang GF. *Appl Catal B-Environ*, 2019, 254: 321–328
12 Sachs M, Sprick RS, Pearce D, Hillman SAJ, Monti A, Guilbert AAY, Brownbill NJ, Dimitrov S, Shi X, Blanc F, Zwijnenburg MA, Nelson J, Durrant JR, Cooper AI. *Nat Commun*, 2018, 9: 4968
13 Sprick RS, Bonillo B, Clowes R, Guiglion P, Brownbill NJ, Slater BJ, Blanc F, Zwijnenburg MA, Adams DJ, Cooper AI. *Angew Chem Int Ed*, 2016, 55: 1792–1796
14 Sprick RS, Aitchison CM, Berardo E, Turcani L, Wilbraham L, Alston BM, Jelfs KE, Zwijnenburg MA, Cooper AI. *J Mater Chem A*, 2018, 6: 11994–12003
15 Lan ZA, Zhang G, Chen X, Zhang Y, Zhang KAI, Wang X. *Angew Chem Int Ed*, 2019, 58: 10236–10240
16 Park JH, Ko KC, Park N, Shin HW, Kim E, Kang N, Hong Ko J, Lee SM, Kim HJ, Ahn TK, Lee JY, Son SU. *J Mater Chem A*, 2014, 2: 7656–7661
17 Guo L, Niu Y, Xu H, Li Q, Razzaque S, Huang Q, Jin S, Tan B. *J Mater Chem A*, 2018, 6: 19775–19781
18 Li L, Fang W, Zhang P, Bi J, He Y, Wang J, Su W. *J Mater Chem A*, 2016, 4: 12402–12406
19 Wang Y, Vogel A, Sachs M, Sprick RS, Wilbraham L, Moniz SJA, Godin R, Zwijnenburg MA, Durrant JR, Cooper AI, Tang J. *Nat Energy*, 2019, 4: 746–760
20 Dai C, Liu B. *Energy Environ Sci*, 2020, 13: 24–52
21 Banerjee T, Gottschling K, Savasci G, Ochsenfeld C, Lotsch BV. *ACS Energy Lett*, 2018, 3: 400–409
22 Zhao C, Chen Z, Shi R, Yang X, Zhang T. *Adv Mater*, 2020, 32: 1907296
23 Zhao D, Dong CL, Wang B, Chen C, Huang YC, Diao Z, Li S, Guo L, Shen S. *Adv Mater*, 2019, 31: 1903545
24 Ye H, Wang Z, Yu F, Zhang S, Kong K, Gong X, Hua J, Tian H. *Appl Catal B-Environ*, 2020, 267: 118577
25 Yu F, Wang Z, Zhang S, Yun K, Ye H, Gong X, Hua J, Tian H. *Appl*

Catal B-Environ, 2018, 237: 32–42
26 Yu F, Wang Z, Zhang S, Ye H, Kong K, Gong X, Hua J, Tian H. *Adv Funct Mater*, 2018, 28: 1804512
27 Yu H, Xue Y, Hui L, Zhang C, Li Y, Zuo Z, Zhao Y, Li Z, Li Y. *Adv Mater*, 2018, 30: 1707082
28 Qi Y, Chen S, Cui J, Wang Z, Zhang F, Li C. *Appl Catal B-Environ*, 2018, 224: 579–585
29 Zhang X, Xiao J, Hou M, Xiang Y, Chen H. *Appl Catal B-Environ*, 2018, 224: 871–876
30 Wang L, Zheng X, Chen L, Xiong Y, Xu H. *Angew Chem Int Ed*, 2018, 57: 3454–3458
31 Chen X, Wang J, Chai Y, Zhang Z, Zhu Y. *Adv Mater*, 2021, 33: 2007479
32 Sachs M, Cha H, Kosco J, Aitchison CM, Francàs L, Corby S, Chiang CL, Wilson AA, Godin R, Fahey-Williams A, Cooper AI, Sprick RS, McCulloch I, Durrant JR. *J Am Chem Soc*, 2020, 142: 14574–14587
33 Sprick RS, Chen Z, Cowan AJ, Bai Y, Aitchison CM, Fang Y, Zwijnenburg MA, Cooper AI, Wang X. *Angew Chem Int Ed*, 2020, 59: 18695–18700
34 Hu J, Li S, Chu J, Niu S, Wang J, Du Y, Li Z, Han X, Xu P. *ACS Catal*, 2019, 9: 10705–10711
35 Zhong Z, Li R, Lin W, Xu X, Tian X, Li X, Chen X, Kang L. *Appl Catal B-Environ*, 2020, 260: 118135
36 Lei F, Sun Y, Liu K, Gao S, Liang L, Pan B, Xie Y. *J Am Chem Soc*, 2014, 136: 6826–6829
37 Zhang B, Wang L, Zhang Y, Ding Y, Bi Y. *Angew Chem Int Ed*, 2018, 57: 2248–2252
38 Ye H, Wang Z, Yang Z, Zhang S, Gong X, Hua J. *J Mater Chem A*, 2020, 8: 20062–20071
39 Kresse G, Furthmüller J. *Phys Rev B*, 1996, 54: 11169–11186
40 Blöchl PE. *Phys Rev B*, 1994, 50: 17953–17979
41 Perdew JP, Burke K, Ernzerhof M. *Phys Rev Lett*, 1996, 77: 3865–3868
42 Teter MP, Payne MC, Allan DC. *Phys Rev B*, 1989, 40: 12255–12263
43 Dai C, Xu S, Liu W, Gong X, Panahandeh-Fard M, Liu Z, Zhang D, Xue C, Loh KP, Liu B. *Small*, 2018, 14: 1801839
44 Zhang W, Ma J, Xiong L, Jiang HY, Tang J. *ACS Appl Energy Mater*, 2020, 3: 5927–5936
45 Zhou J, Wang Y, Cui Z, Hu Y, Hao X, Wang Y, Zou Z. *Appl Catal B-Environ*, 2020, 277: 119228
46 Lin Y, Su W, Wang X, Fu X, Wang X. *Angew Chem Int Ed*, 2020, 59: 20919–20923
47 Lin Z, Zhao Y, Luo J, Jiang S, Sun C, Song S. *Adv Funct Mater*, 2020, 30: 1908797
48 Shen R, Xie J, Lu X, Chen X, Li X. *ACS Sustain Chem Eng*, 2018, 6: 4026–4036
49 Xiang Q, Cheng F, Lang D. *ChemSusChem*, 2016, 9: 996–1002
50 Chemelewski WD, Lee HC, Lin JF, Bard AJ, Mullins CB. *J Am Chem Soc*, 2014, 136: 2843–2850
51 Seabold JA, Choi KS. *J Am Chem Soc*, 2012, 134: 2186–2192
52 Yan J, Li P, Ji Y, Bian H, Li Y, Liu SF. *J Mater Chem A*, 2017, 5: 21478–21485
53 Bai Y, Nakagawa K, Cowan AJ, Aitchison CM, Yamaguchi Y, Zwijnenburg MA, Kudo A, Sprick RS, Cooper AI. *J Mater Chem A*, 2020, 8: 16283–16290
54 Yue J, Jiang X, Yu A. *J Nanopart Res*, 2011, 13: 3961–3974